GENETICS

CRISPR-Cas9 corrects Duchenne muscular dystrophy exon 44 deletion mutations in mice and human cells

Yi-Li Min[1,2], Hui Li[1,2], Cristina Rodriguez-Caycedo[1,2], Alex A. Mireault[1,2], Jian Huang[3], John M. Shelton[3], John R. McAnally[1,2], Leonela Amoasii[1,2,4], Pradeep P. A. Mammen[2,3], Rhonda Bassel-Duby[1,2], Eric N. Olson[1,2]*

Mutations in the dystrophin gene cause Duchenne muscular dystrophy (DMD), which is characterized by lethal degeneration of cardiac and skeletal muscles. Mutations that delete exon 44 of the dystrophin gene represent one of the most common causes of DMD and can be corrected in ~12% of patients by editing surrounding exons, which restores the dystrophin open reading frame. Here, we present a simple and efficient strategy for correction of exon 44 deletion mutations by CRISPR-Cas9 gene editing in cardiomyocytes obtained from patient-derived induced pluripotent stem cells and in a new mouse model harboring the same deletion mutation. Using AAV9 encoding Cas9 and single guide RNAs, we also demonstrate the importance of the dosages of these gene editing components for optimal gene correction in vivo. Our findings represent a significant step toward possible clinical application of gene editing for correction of DMD.

INTRODUCTION

Duchenne muscular dystrophy (DMD), caused by mutations in the dystrophin gene, is characterized by degeneration of cardiac and skeletal muscles, loss of ambulation, and premature death (*1*). Dystrophin is a massive protein (>3600 amino acids), which stabilizes muscle membranes by tethering the actin cytoskeleton to the inner surface of the sarcolemma (*2*, *3*). Thousands of mutations that prevent dystrophin production have been identified in patients with DMD (*4*). These mutations cluster in hotspot regions of the gene that can, in principle, be bypassed by various exon skipping strategies to restore the dystrophin open reading frame (*5*). To date, however, there has been no effective long-term therapy for this disease, and the only drug approved by the Food and Drug Administration for the treatment of DMD allows for restoration of <1% of the normal level of dystrophin protein after extended treatment (*6*). Thus, there remains a major unmet medical need for new strategies to correct the underlying cause of DMD—genetic mutations in the dystrophin gene.

A substantial challenge in the development of DMD therapies has been the lack of animal models harboring the most common human mutations. Because the mouse and human dystrophin genes both contain 79 exons with highly conserved exon splicing patterns, results obtained in mouse models of the disease can be extrapolated to the human condition. One of the most common deletions in patients with DMD eliminates exon 50 in the rod domain of dystrophin, which places exon 51 out of frame with preceding exons (*4*, *7*–*10*). We recently described the rescue of mice and dogs lacking exon 50 by injection of two adeno-associated viruses of serotype 9 (AAV9) encoding the CRISPR-Cas9 gene and single guide RNAs (sgRNAs) that allow skipping or reframing of exon 51 and restoration of dystrophin expression (*11*, *12*).

The second most common mutational hotspot in the dystrophin gene includes exon 44, which disrupts the open reading frame in surrounding exons (*4*, *7*–*9*). Here, we describe the creation of a new mouse model of DMD with exon 44 deletion, and we present two strategies for correction of this mutation by CRISPR-Cas9–mediated skipping of surrounding exons. These mice represent an important tool for the testing and optimization of diverse therapies for DMD. We also show that sgRNAs, unexpectedly, are limiting for optimal gene editing in vivo and that editing efficiency can be enhanced ~10-fold by optimizing the dose of AAVs encoding Cas9 and sgRNAs. Our findings highlight the potential of gene editing to permanently eradicate mutations that cause DMD, thereby preventing the pathogenic sequelae of this disease.

RESULTS

Correction of a DMD exon 44 deletion in patient-derived induced pluripotent stem cells

We generated patient-derived induced pluripotent stem cells (iPSCs) from a patient with DMD lacking exon 44 of the dystrophin gene (*DMD*) and from the patient's brother with a normal dystrophin gene as a healthy control (Fig. 1A). Deletion of exon 44 (ΔEx44) disrupts the open reading frame of dystrophin by causing splicing of exon 43 to exon 45 and introducing a premature termination codon (Fig. 1B). The reading frame can be restored by using CRISPR-Cas9 gene editing to skip exon 43, which allows splicing between exons 42 and 45, or to skip exon 45, which allows splicing between exons 43 and 46. Alternatively, reframing of exon 43 or 45 can restore the protein reading frame by inserting one nucleotide (+3n+1 insertion) or deleting two nucleotides (+3n−2 deletion).

We selected sgRNAs that permit deletion of the splice acceptor or donor sites of exons 43 and 45, thereby allowing splicing between surrounding exons to recreate in-frame dystrophin. For editing exon 43, we designed four 20–nucleotide (nt) sgRNAs (G1, G2, G3, and G4) directed against sequences near the 5′ and 3′ boundaries of the splice junctions of exon 43 (Fig. 1C). For exon 45, we observed

[1]Department of Molecular Biology, Hamon Center for Regenerative Science and Medicine, University of Texas Southwestern Medical Center, 5323 Harry Hines Boulevard, Dallas, TX 75390, USA. [2]Sen. Paul D. Wellstone Muscular Dystrophy Cooperative Research Center, University of Texas Southwestern Medical Center, 5323 Harry Hines Boulevard, Dallas, TX 75390, USA. [3]Department of Internal Medicine, University of Texas Southwestern Medical Center, 5323 Harry Hines Boulevard, Dallas, TX 75390, USA. [4]Exonics Therapeutics, 490 Arsenal Way, Watertown, MA 02472, USA.
*Corresponding author. Email: eric.olson@utsouthwestern.edu

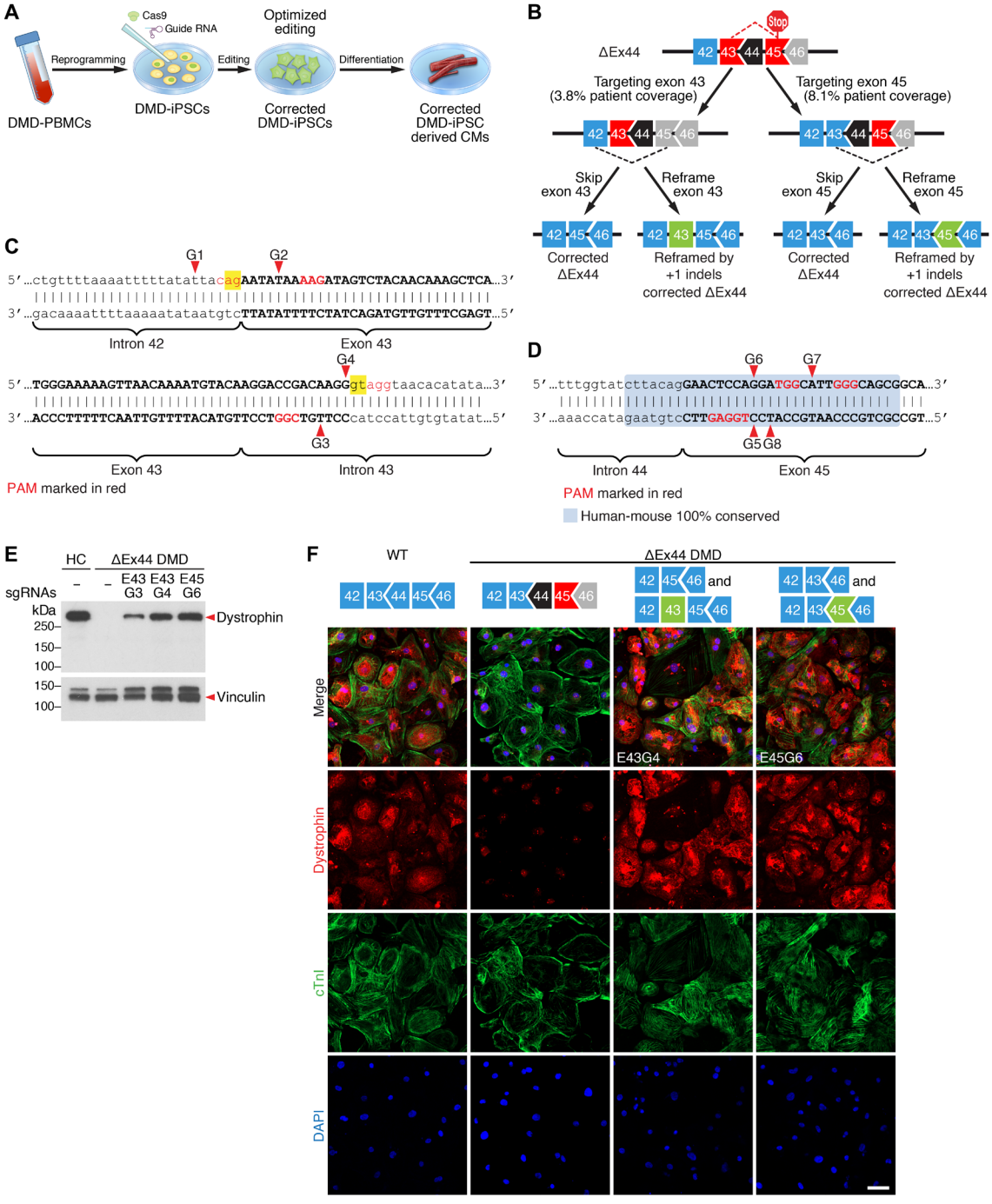

Fig. 1. Exon 44–deleted DMD patient iPSC-derived cardiomyocytes express dystrophin after CRISPR-Cas9–mediated genome editing. (**A**) Schematic of the procedure for deriving and editing patient with DMD–derived iPSCs and iPSC-CMs. (**B**) Gene editing strategy for *DMD* exon 44 deletion. Deletion of exon 44 (black) results in splicing of exons 43 to 45, generating an out-of-frame stop mutation of dystrophin. Disruption of the splice junction of exon 43 or exon 45 results in splicing of exons 42 to 45 or exons 43 to 46, respectively, and restores the protein reading frame. The protein reading frame can also be restored by reframing exon 43 or 45 (green). (**C**) Sequence of sgRNAs targeting exon 43 splice acceptor and donor sites in the human *DMD* gene. The protospacer adjacent motif (PAM) (denoted as red nucleotides) of the sgRNAs is located near the exon 43 splice junctions. Exon sequence is represented by letters in bold uppercase. Intron sequence is represented by letters in lowercase. Arrowheads show sites of Cas9 DNA cutting with each sgRNA. Splice acceptor and donor sites are shaded in yellow. (**D**) Sequence of sgRNAs targeting exon 45 splice acceptor site in the human *DMD* gene. The PAM (denoted as red nucleotides) of the sgRNAs is located near the exon 45 splice acceptor site. The human and mouse conserved sequence is shaded in light blue. Exon sequence is represented by letters in bold uppercase. Intron sequence is represented by letters in lowercase. (**E**) Western blot analysis shows restoration of dystrophin expression in exon 43–edited (E43) and exon 45–edited (E45) ΔEx44 patient iPSC-CMs with sgRNAs (G) 3, 4, and 6, as indicated. Vinculin is the loading control. HC indicates iPSC-CMs from a healthy control. The second lane is the unedited ΔEx44 patient iPSC-CMs. (**F**) Immunostaining shows restoration of dystrophin expression in exon 43–edited and exon 45–edited ΔEx44 patient iPSC-CMs. Dystrophin is shown in red. Cardiac troponin I is shown in green. Nuclei are marked by 4′,6-diamidino-2-phenylindole (DAPI) stain in blue. Scale bar, 50 μm.

that the intron-exon junction of the splice acceptor site is contained within a 33–base pair (bp) region that is identical in the human and mouse genomes, allowing exon skipping strategies to be interchanged between the two species (fig. S1A). We generated four 18- to 20-nt sgRNAs (G5, G6, G7, and G8) to target the 5′ boundary of exon 45 within the conserved region of the human and mouse genomes (Fig. 1D). By the mismatch-specific T7 endonuclease I (T7E1) assay, we compared the sgRNAs for their ability to direct Cas9-mediated gene editing in human 293 cells (fig. S1B). Two of four sgRNAs for exon 43 efficiently edited the targeted region, and all four sgRNAs for exon 45 generated precise cuts at the conserved region (fig. S1C). We concurrently tested the editing activity of the same four sgRNAs for exon 45 in mouse 10T½ cells and confirmed the effectiveness of the four sgRNAs in both the human and mouse genomes (fig. S1C).

sgRNAs with the highest gene editing activity based on the T7E1 assays were then tested for the ability to efficiently edit the corresponding exons in patient-derived iPSCs lacking exon 44 (referred to as ΔEx44). A single plasmid encoding optimized sgRNAs (G3 or G4 for exon 43, or G6 for exon 45) and *Streptococcus pyogenes* Cas9 (*Sp*Cas9) was introduced into ΔEx44 patient-derived iPSCs by electroporation, and the edited iPSCs were differentiated into cardiomyocytes (iPSC-CMs). Dystrophin expression was assessed by Western blot analysis and immunostaining, confirming restoration of dystrophin protein expression in edited ΔEx44 iPSC-CMs (Fig. 1, E and F). Levels of dystrophin protein expression in ΔEx44 iPSC-CMs edited with sgRNAs G4 and G6 were approximately comparable to those seen in healthy control iPSC-CMs (Fig. 1E).

Because of the high efficiency of editing in the T7E1 assay and the complete conservation of sequence between human and mouse genomes, we chose to use sgRNA G6 to derive single clones of ΔEx44 iPSCs that were edited within exon 45. Thirty-four single clones were isolated and expanded. Sequence analysis of the clones showed exon skipping events in 3 of 34 clones, and dystrophin reframing by either +3n+1 or +3n−2 in 13 of 34 clones (fig. S1D). Western blot analysis confirmed the restoration of dystrophin expression in three of the CRISPR-Cas9 corrected clones (fig. S1E).

Generation of mice with a DMD exon 44 deletion

To optimize gene editing for correction of an exon 44 deletion in vivo, we generated a mouse model bearing an exon 44 deletion in the *Dmd* gene by CRISPR-Cas9 gene editing (Fig. 2A). We injected zygotes of C57BL/6 mice with two sgRNAs that target the introns flanking exon 44 and implanted the zygotes into surrogate female mice (fig. S2A). An F0 founder with a 908-bp deletion that eliminated exon 44 was chosen for further studies. These ΔEx44 DMD mice contain one of the most common deletions responsible for DMD in humans. In principle, correction of exon 44 deletions by gene editing of surrounding exons could potentially restore the reading frame of dystrophin in ~12% of patients with DMD. Deletion of exon 44 was confirmed by reverse transcription polymerase chain reaction (RT-PCR) analysis (Fig. 2B). Sequencing of the RT-PCR products using primers for sequences in exons 43 and 46 confirmed the removal of exon 44 in these mice (Fig. 2C). At 4 weeks of age, immunostaining of the tibialis anterior (TA) muscle, diaphragm, and heart in the ΔEx44 DMD mice showed complete absence of dystrophin protein expression (Fig. 2D). Western blot analysis confirmed loss of dystrophin protein (Fig. 2E). Fibrosis, inflammatory infiltration, and regenerative fibers with centralized nuclei were observed in 4-week-old ΔEx44 DMD mice, indicative of a severe muscular dystrophy phenotype (Fig. 2F and fig. S2B). Serum creatine kinase (CK) levels in the ΔEx44 DMD mice were elevated 22-fold compared with wild-type (WT) littermates, similar to *mdx* mice, an established DMD mouse model (Fig. 2G).

Shear force generated during muscle contraction leads to muscle membrane tearing in muscle lacking dystrophin, eventually causing myofiber degeneration and muscle fibrosis (*13*). Fibrotic tissue increases muscle stiffness and compromises contractility of muscles. To further analyze muscle function of ΔEx44 DMD mice, we measured maximal tetanic force in the extensor digitorum longus (EDL) muscle ex vivo. Compared with WT littermates at 4 weeks of age, ΔEx44 DMD mice showed an ~50% decrease in the specific and absolute tetanic force in the EDL muscle (Fig. 2, H and I). A similar decrease in muscle strength was observed by grip strength analysis in 8-week-old ΔEx44 DMD mice (Fig. 2J).

Correction of DMD exon 44 deletion in mice by intramuscular AAV9 delivery of gene editing components

To deliver *Sp*Cas9 and sgRNA in vivo, we used AAV9 to package the gene editing components. AAV9 is a single-stranded DNA virus that displays tropism to both skeletal muscle and heart and has been used in numerous clinical trials (*14*–*17*). To further achieve muscle-specific gene editing, we used the creatine kinase 8 (CK8e) regulatory cassette that combines key elements of the enhancer and promoter regions of the muscle CK gene to drive *Sp*Cas9 expression in skeletal muscle and heart (*18*, *19*). For the delivery of sgRNA, we used three RNA polymerase III promoters (U6, H1, and 7SK) to express three copies of the sgRNA (fig. S3A) (*20*).

We first compared the efficiency of gene editing with different expression constructs encoding Cas9 and sgRNAs. The PX458 plasmid encodes both editing components (*21*), whereas we used two AAV expression plasmids to express Cas9 and three copies of the sgRNA that targeted exon 45 in mouse C2C12 muscle cells. By using the T7E1 assay, we observed comparable editing efficiency with both constructs (fig. S3B). Among the two sgRNAs tested, G6 showed better cutting efficiency than G5, consistent with the observations in mouse 10T½ cells and human 293 cells (fig. S1C).

To validate the efficacy of the single-cut gene editing strategy in the ΔEx44 DMD mouse model, we performed localized intramuscular injection of AAV9 encoding *Sp*Cas9 (AAV-Cas9) and AAV9 encoding sgRNA (AAV-G5 or AAV-G6) in the TA muscle of postnatal day 12 (P12) mice. As a control group, WT and ΔEx44 DMD mice were injected with AAV-Cas9 without AAV-sgRNA. In initial studies, 50 μl of AAV9 (1×10^{12} vg/ml) was injected per leg, containing equal amounts of AAV-Cas9 and AAV-G5 or AAV-G6. Three weeks after the intramuscular injection, we collected the TA muscles for analysis. In vivo gene editing by AAV-G5 and AAV-G6 was compared by the T7E1 assay and RT-PCR of the targeted region (Fig. 3A and fig. S3C). Gene editing with AAV-G6 showed higher efficiency based on DNA cutting in vivo (fig. S3C). RT-PCR with primers that amplify the region from exon 43 to exon 46 revealed deletion of exon 45 in the TA muscle injected with AAV-Cas9 and AAV-G6 (Fig. 3A). This allows exon 43 to skip exon 45 and directly splice to exon 46 when processing the pre-mRNA. As a result, the alternate mRNA enables the production of a truncated dystrophin protein in the corrected TA muscle of ΔEx44 DMD mice.

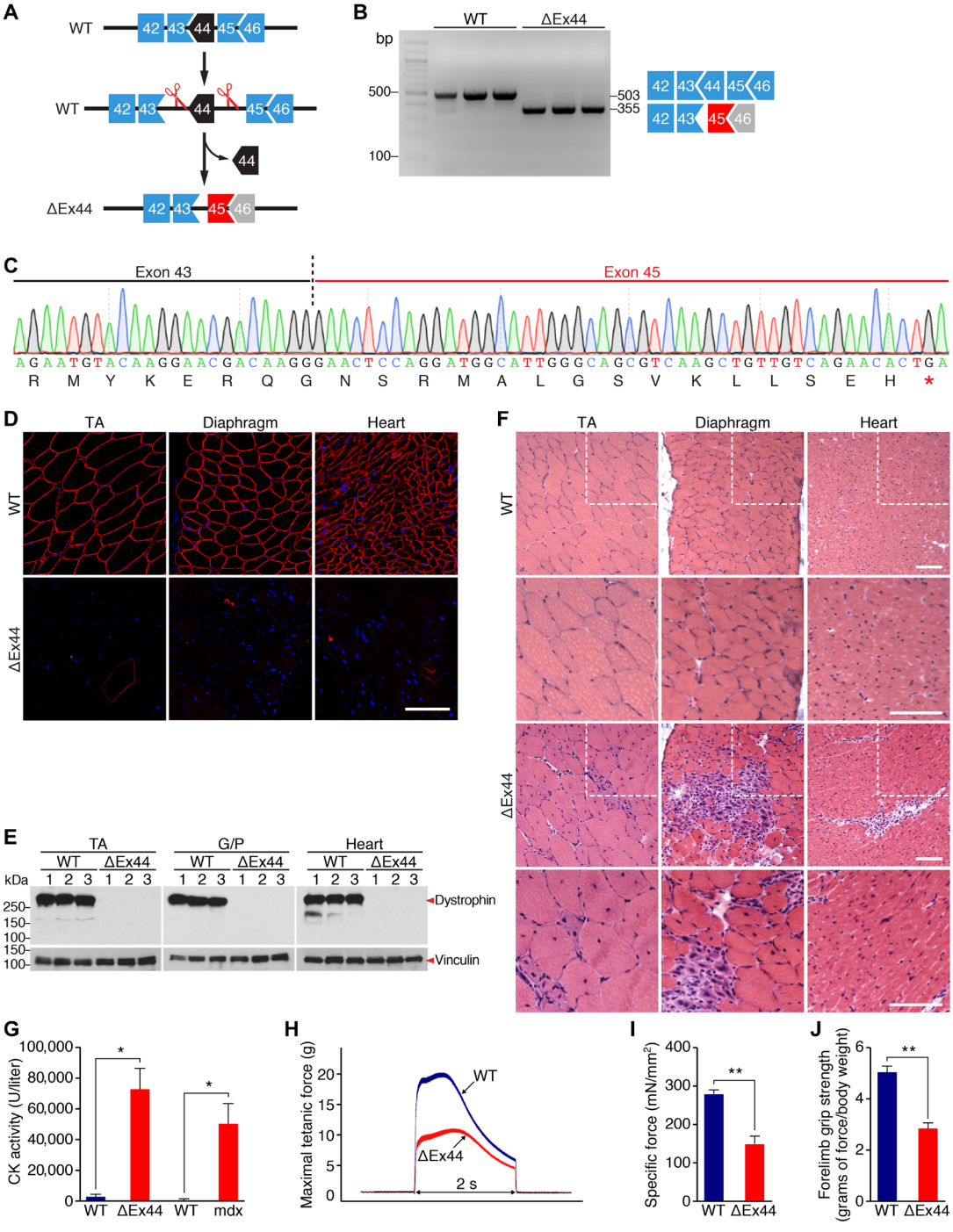

Fig. 2. Generation of mice with a DMD exon 44 deletion. (**A**) CRISPR-Cas9 editing strategy used for generation of mice with exon 44 deletion (ΔEx44). Exon 45 (red) is out of frame with exon 43. (**B**) RT-PCR analysis of TA muscles to validate deletion of exon 44. RT-PCR primers were in exons 43 and 46, and the amplicon size is 503 bp for WT mice and 355 bp for ΔEx44 DMD mice. RT-PCR products are schematized on the right ($n = 3$). (**C**) Sequencing of RT-PCR products from ΔEx44 DMD mouse muscle confirmed deletion of exon 44 and generation of a premature stop codon in exon 45, indicated by red asterisk. (**D**) Dystrophin staining of the TA, diaphragm, and heart of WT and ΔEx44 DMD mice. Dystrophin is shown in red. Nuclei are marked by DAPI stain in blue. Scale bar, 100 μm. (**E**) The Western blot analysis shows loss of dystrophin expression in the TA, gastrocnemius/plantaris (G/P) muscle, and heart of ΔEx44 mice. Vinculin is the loading control ($n = 3$). (**F**) H&E staining of the TA, diaphragm, and heart. Note extensive inflammatory infiltrate and centralized myonuclei in ΔEx44 sections. Inset boxes indicate areas of magnification shown below. Scale bars, 50 μm. (**G**) Serum creatine kinase (CK), a marker of muscle damage and membrane leakage, was measured in WT (C57BL/6 and C57BL/10), ΔEx44, and *mdx* mice. Data are represented as mean ± SEM. Unpaired Student's *t* test was performed. $^{*}P < 0.005$ ($n = 6$). (**H**) Representative trace of maximal tetanic force of EDL muscles in WT (blue) and ΔEx44 mice (red). $P < 0.005$ ($n = 6$). (**I**) Specific force of EDL muscles in WT (blue) and ΔEx44 mice (red). Data are represented as mean ± SEM. Unpaired Student's *t* test was performed. $^{**}P < 0.001$ ($n = 6$). (**J**) Forelimb grip strength analysis of WT and ΔEx44 mice. Data are represented as mean ± SEM. Unpaired Student's *t* test was performed. $^{**}P < 0.001$ ($n = 6$).

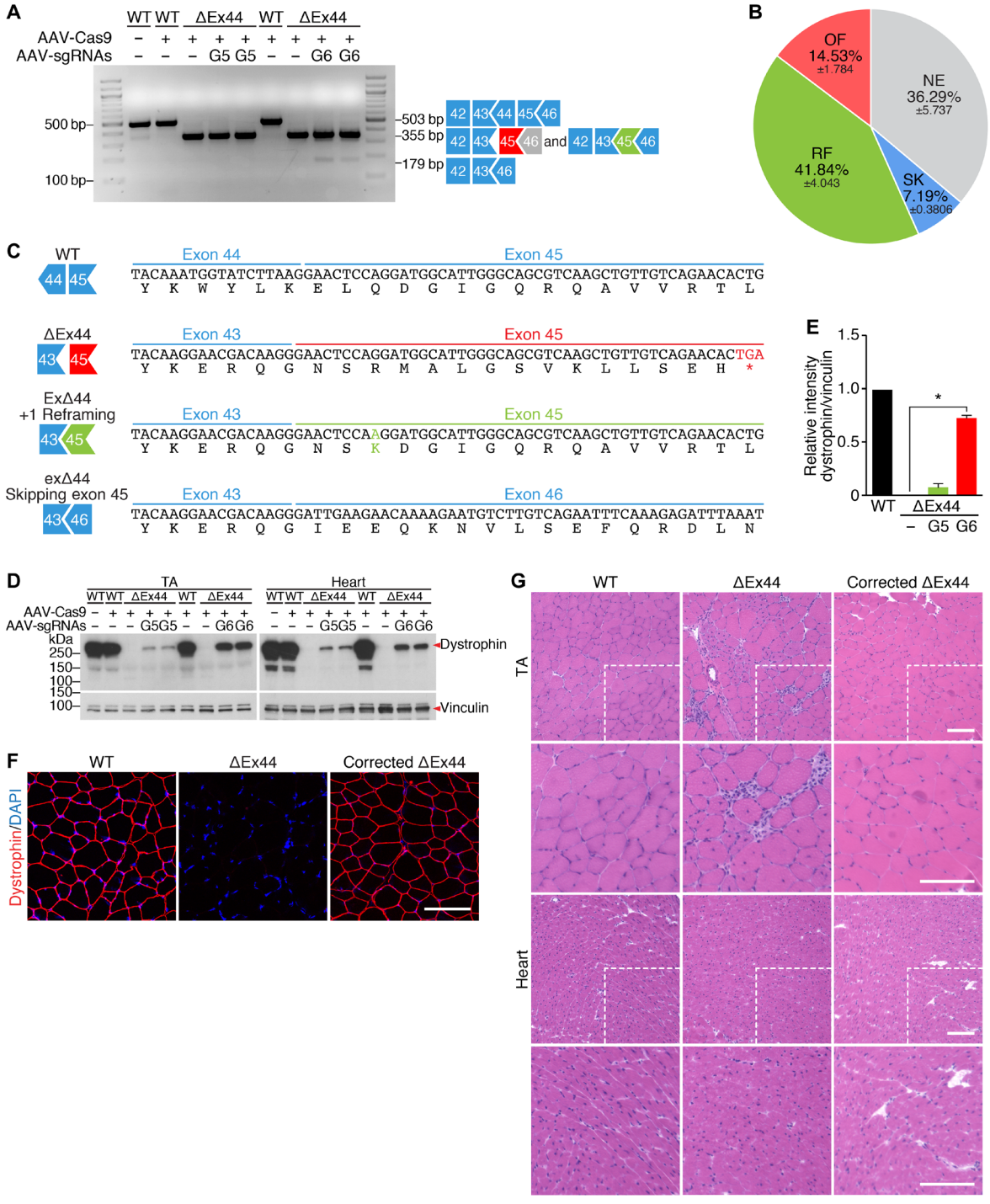

Fig. 3. Correction of *Dmd* exon 44 deletion in mice by intramuscular AAV9 delivery of gene editing components. (**A**) RT-PCR analysis of TA muscles from WT and ΔEx44 mice 3 weeks after intramuscular injection of gene editing components carried by AAV9. Lower dystrophin bands (179 bp) indicate skipping of exon 45. (**B**) Pie chart showing percentage of events detected at exon 45 after AAV-Cas9 and AAV-G6 treatment using RT-PCR sequence analysis of TOPO-TA generated clones. RT-PCR products were divided into four groups: NE, not edited; SK, exon 45 skipped; RF, reframed; and OF, out of frame. Data are represented as mean ± SEM ($n = 3$). (**C**) Sequences of RT-PCR products of WT, ΔEx44, and corrected ΔEx44 mice. In-frame sequences are shown in blue, including WT and exon 45–skipped sequences. Reframed sequence is shown in green, and out-of-frame sequence is shown in red. (**D**) Western blot analysis shows restoration of dystrophin expression in the TA muscle and heart of ΔEx44 mice. Vinculin is the loading control. (**E**) Quantification of the Western blot analysis in the TA muscle. Relative dystrophin intensity was calibrated with vinculin internal control. Data are represented as mean ± SEM. Unpaired Student's *t* test was performed. *$P < 0.005$ ($n = 3$). (**F**) Immunostaining shows restoration of dystrophin in the TA muscle of ΔEx44 mice 3 weeks after intramuscular injection of gene editing components carried by AAV9. Dystrophin is shown in red. Nuclei are marked by DAPI stain in blue. Scale bar, 100 μm ($n = 3$). (**G**) H&E staining of the TA and heart in WT, ΔEx44, and corrected ΔEx44 mice. Inset boxes indicate areas of magnification shown below. Scale bars, 50 μm ($n = 3$).

To further evaluate the mutations generated by gene editing, we performed topoisomerase-based thymidine to adenosine (TOPO-TA) cloning using the RT-PCR amplification products and sequenced the cDNA products. Sequencing results demonstrated that 7% of sequenced clones represented exon 45–skipped cDNA products, and 42% of sequenced clones contained a single adenosine (A) insertion in exon 45 that resulted in reframing of dystrophin protein (Fig. 3, B and C). The predominance of reframing explains the high abundance of the RT-PCR band at 355 bp and the lower abundance of the smaller RT-PCR product at 179 bp, which reflects exon skipping (Fig. 3A).

Genomic and cDNA amplicon deep sequencing on the target region of the TA muscles with AAV-G6 intramuscular injection also confirmed that 9.8% of mutations at the genomic level and 35.7% of mutations at the mRNA level contain a single A insertion at the cutting site after gene editing with AAV-G6 (fig. S3, D and E). This single A insertion leads to reframing of exon 45 and restores the dystrophin protein reading frame. We also observed minor AAV inverted terminal repeat (ITR) integration events at the cutting site, with a frequency of 0.21% at the genomic level (fig. S3D) and 1.15% at the mRNA level (fig. S3E).

To evaluate dystrophin protein restoration after intramuscular injection with AAV-Cas9 and AAV-G5 or AAV-G6, we performed Western blot analysis on the TA muscle and the heart (Fig. 3D). We observed restoration of dystrophin protein expression to 74% of the WT level in edited TA muscles of ΔEx44 DMD mice (Fig. 3E). Although the injection was localized to the TA muscle, we observed expression of dystrophin in the heart at 21% of the WT level (Fig. 3D). This suggests leakage of AAV into the circulation and delivery of the gene editing components to the heart. Immunostaining showed that dystrophin protein expression was restored in 99% of the myofibers in TA muscle injected with AAV-Cas9 and AAV-G6 (Fig. 3F and fig. S3F). Histological analysis and hematoxylin and eosin (H&E) staining showed a pronounced reduction in fibrosis, necrotic myofibers, and regenerating fibers with central nuclei, indicating amelioration of the abnormalities associated with muscular dystrophy in the TA muscle 3 weeks after AAV9-Cas9 and AAV-G6 injection (Fig. 3G).

On the basis of the CRISPR design tools (http://crispr.mit.edu/ and https://benchling.com/), we determined the top 10 potential off-target sites, and on the basis of sequencing analysis, we did not detect off-target effects at these sites (fig. S4). The T7E1 analysis confirmed the absence of off-target cutting in the top 10 potential off-target sites, and DNA sequencing of the isolated genomic PCR amplification products spanning the potential off-target sites confirmed the absence of sgRNA/Cas9-mediated mutations at the predicted sites (fig. S4A). In addition, we performed genomic amplicon deep sequencing of the top 10 predicted off-target sites within protein-coding exons. None of these sites showed significant sequence alterations (fig. S4, B and C).

Systemic delivery of AAV9 expressing gene editing components rescues dystrophin expression in ΔEx44 mice

To achieve body-wide rescue of the disease phenotype in ΔEx44 DMD mice, we delivered AAV-Cas9 and AAV-G6 systemically through intraperitoneal injection. AAV-Cas9 was injected at a dosage of 5×10^{13} vg/kg. Multiple ratios of AAV-G6 to AAV-Cas9 were tested to determine whether there might be an optimal ratio of the viruses for maximal systemic editing efficiency. Four weeks after injection, we assessed dystrophin protein expression in several muscle tissues, including TA muscle of the hindlimb, triceps of the forelimb, diaphragm, and cardiac muscle. By immunostaining, we observed dystrophin expression in 94, 90, and 95% of myofibers in the TA, triceps, and diaphragm, respectively, and in 94% of cardiomyocytes when ΔEx44 mice were injected with a 1:10 ratio of AAV-Cas9:AAV-G6 (5×10^{13} vg/kg of AAV-Cas9 and 5×10^{14} vg/kg of AAV-G6) (Fig. 4A and fig. S5). The restoration of dystrophin protein in skeletal muscles correlated with the dosage of AAV-G6 delivered through intraperitoneal injection. In contrast, in the heart, dystrophin-positive cardiomyocytes were seen at a low dosage of AAV-G6 and remained consistent at higher dosages. Western blot analysis of the same muscle groups after systemic delivery showed similar trends of dystrophin correction (Fig. 4B and fig. S6). At every ratio of AAV-Cas9:AAV-G6 tested by systemic delivery, the cardiac muscle showed higher dystrophin restoration than the skeletal muscle. Correction of the cardiac muscle reached 82% when injected at a 1:1 ratio of AAV-Cas9:AAV-G6 and increased an additional 12% at a 1:10 ratio. In contrast, we observed an increase in dystrophin-expressing myofibers from 10 to 94% when the sgRNA was increased. H&E and Picrosirius red staining showed that histopathologic hallmarks of muscular dystrophy, such as regenerated fibers with central nuclei, were diminished in the TA, diaphragm, and triceps muscles at 4 weeks after AAV-Cas9 and AAV-G6 delivery (figs. S7 and S8A). Quantitative analysis of the distribution of muscle fiber cross-sectional area showed an improvement in the TA muscle at 4 weeks after delivery of AAV-Cas9:AAV-G6 at 1:5 and 1:10 ratios (fig. S8B).

To further assess systemic delivery of AAV-Cas9 in the presence of different amounts of AAV-G6, we performed Western blot analysis to evaluate the amount of Cas9 protein expressed in the muscles. Although we kept the total AAV-Cas9 dosage constant (5×10^{13} vg/kg), the mice that received higher doses of AAV-G6 showed greater expression of Cas9 protein in corrected muscles (Fig. 4B and fig. S6). Quantitative polymerase chain reaction (qPCR) analysis of Cas9 mRNA in muscle groups comparing low and high doses of AAV-G6 revealed increased Cas9 mRNA expression in the skeletal muscle in the presence of high doses of AAV-G6 (fig. S8, C and D). These results indicate that Cas9 expression is affected by the amount of sgRNA present, and thus, sgRNA is limiting for optimal gene editing in vivo. These results also suggest that the extent of dystrophin restoration and muscle recovery may provide an environment that favors Cas9 expression.

To examine the effect of dystrophin restoration on muscle function in systemically corrected ΔEx44 DMD mice, we performed electrophysiology on the EDL muscle of ΔEx44 DMD mice at 4 weeks after injection with AAV-Cas9 and AAV-G6. We observed rescue of maximal tetanic force in the EDL muscle of the corrected ΔEx44 DMD mice (Fig. 4C). Improvement of muscle function correlated with increased dystrophin expression and decreased muscle degeneration and was associated with administration of increasing amounts of AAV-G6 relative to AAV-Cas9 (fig. S9). For measurement of muscle-specific force, which is calibrated with the muscle cross-sectional area, we observed an increase in force from 59 to 89% for a 1:5 ratio and to 107% for a 1:10 ratio of AAV-Cas9:AAV-G6 in the EDL muscle of systemically corrected ΔEx44 DMD mice (Fig. 4D). We conclude that systemic delivery of AAV-Cas9 and AAV-G6 efficiently restores dystrophin expression and improves muscle function in corrected ΔEx44 DMD mice, and the amount of

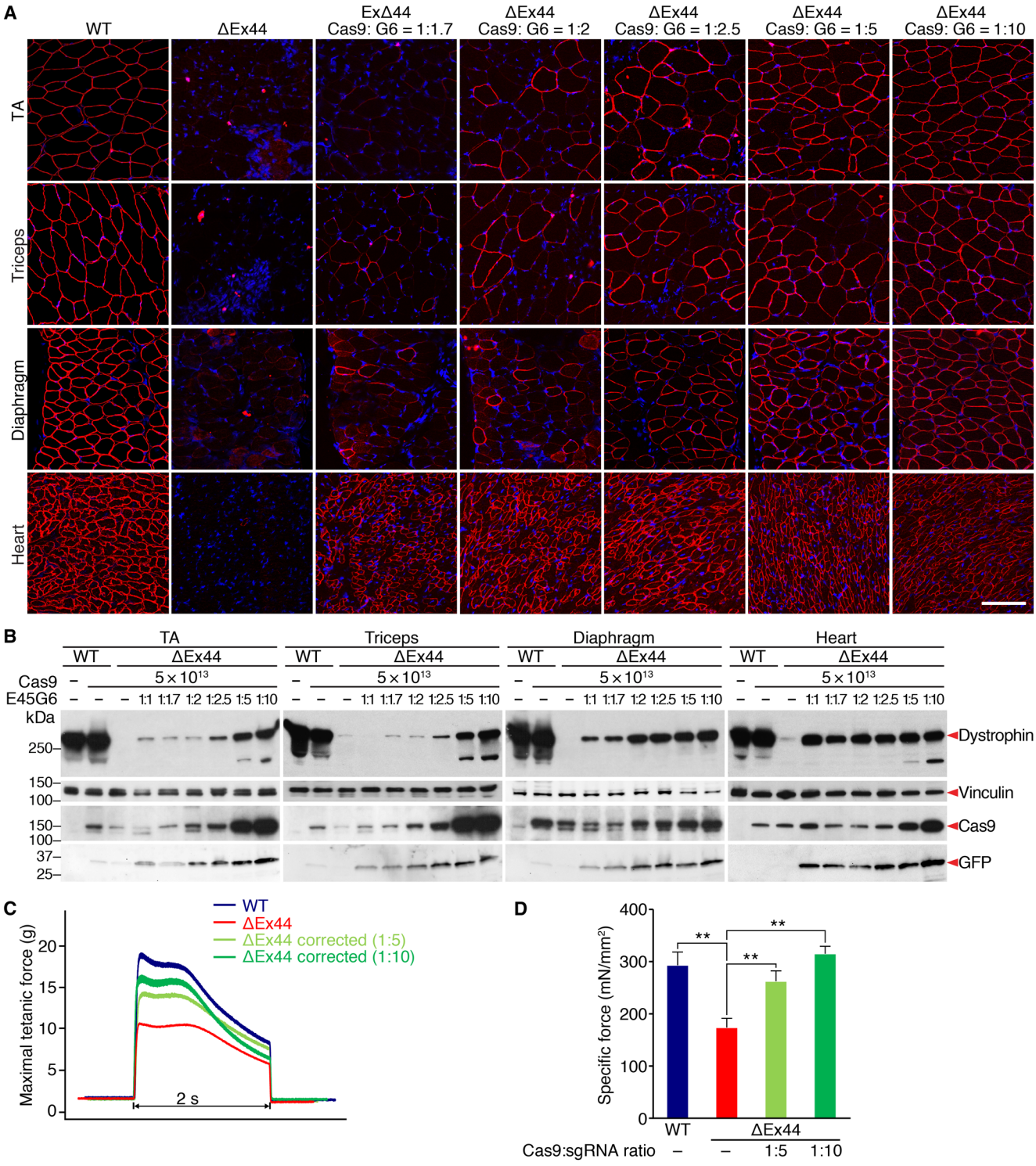

Fig. 4. Systemic AAV9 delivery of gene editing components to ΔEx44 mice rescues dystrophin expression. (**A**) Immunostaining shows restoration of dystrophin in the TA, triceps, diaphragm, and heart of ΔEx44 mice 4 weeks after systemic delivery of AAV-Cas9 and AAV-G6 at the indicated ratios. Dystrophin is shown in red. Nuclei are marked by DAPI stain in blue. Scale bar, 100 μm (**B**) Western blot analysis shows restoration of dystrophin expression in the TA, triceps, diaphragm, and heart of ΔEx44 mice 4 weeks after systemic delivery of AAV-Cas9 and AAV-G6 at the indicated ratios. Vinculin the loading control ($n = 4$). (**C**) Maximal tetanic force of the EDL muscles in WT (blue), ΔEx44 DMD (red), and corrected ΔEx44 DMD (green) mice 4 weeks after systemic delivery of AAV-Cas9 and AAV-sgRNA at 1:5 and 1:10 ratios. $P < 0.005$ ($n = 6$). (**D**) Specific force (mN/mm^2) of the EDL muscles in WT (blue), ΔEx44 DMD (red), and corrected ΔEx44 DMD (green) mice 4 weeks after systemic delivery of AAV-Cas9 and AAV-sgRNA at 1:5 and 1:10 ratios. Data are represented as mean ± SEM. One-way ANOVA was performed, followed by Newman-Keuls post hoc test. $^{**}P < 0.001$ ($n = 6$).

sgRNA delivered to the muscle is critical to the efficiency of genome editing in vivo.

DISCUSSION

Our results establish a new mouse model of DMD lacking exon 44 of the dystrophin gene, representing one of the most prevalent hotspot regions for dystrophin gene mutations in humans. Correction of exon 44 deletions through exon skipping or reframing of surrounding exons could potentially treat ~12% of patients with DMD. These ΔEx44 DMD mice display the hallmarks of DMD, including myocyte degeneration, regeneration, fibrosis, and fatty infiltration of muscle, as well as loss of contractile function, and will provide a platform for testing and optimizing gene editing strategies and other therapies. The dystrophin exon 44 deletion in these mice and the strategy for restoration of dystrophin expression by skipping exon 45 are analogous to the correction strategy using the oligonucleotide casimersen (SRP-4045), developed by Sarepta, which is designed to restore dystrophin expression in patients with exon 44 deletions by masking the splice acceptor site on exon 45. In a recent clinical trial, eteplirsen, an oligonucleotide that allows exon 51 skipping in patients lacking exon 50, was reported to allow the expression of ~0.5% of the normal level of dystrophin, as measured in biopsy samples from treated patients with DMD after approximately 1 year of continuous treatment (*6*). By comparison, we observed ~90% restoration of dystrophin protein expression in all muscles and the heart of mice with exon 44 deletion within 4 weeks of a single systemic dose of gene editing components encoded by AAV9. It has been estimated that only 15 to 30% of normal dystrophin levels could provide therapeutic benefits in patients (*22*, *23*).

We show that the ratio of AAVs encoding sgRNA and Cas9 can have a profound effect on the efficiency of gene correction in vivo. Increasing the ratio of AAV-sgRNA to AAV-Cas9 markedly increases gene correction by single-cut CRISPR. There are several potential explanations to account for these observations: (i) AAV-sgRNA may be limiting in vivo, such that more virus enables greater gene editing. Moreover, because association of Cas9 with sgRNA has been reported to induce a conformational change in Cas9 that potentiates gene editing (*24*), higher levels of sgRNA may ensure higher Cas9 activity in vivo. (ii) sgRNAs are transcribed by RNA polymerase III and are likely to be confined to the nucleus (*25*, *26*). Cas9 protein, derived from translation of Cas9 mRNA in the cytoplasm, can enter nuclei other than those in which the sgRNA was transcribed. Increasing the level of AAV-sgRNA may allow for a higher percentage of nuclei within myofibers to express the sgRNA, thereby enhancing CRISPR-Cas9 genomic editing. (iii) Depletion of sgRNA may occur over time in vivo, and increasing the abundance of sgRNA may ensure continuous editing in myofibers.

When a constant dosage of AAV-Cas9 was administered with higher amounts of AAV-sgRNA, we observed increased Cas9 protein and mRNA expression. Perhaps, the increase in Cas9 expression with sgRNA dosage and the consequent increase in dystrophin restoration lead to a healthier cellular environment for Cas9 expression. The difference in rescue efficiency at different ratios of AAV-sgRNA and AAV-Cas9 potentially correlates with the number of nuclei edited in each cell. Although both cardiac muscle and skeletal muscle are multinucleated, a single cardiomyocyte contains one to four nuclei on average, but one myofiber may contain hundreds of nuclei. Thus, generating dystrophin-expressing myocytes by editing nuclei in one cardiomyocyte is more efficient than in one myofiber. As a result, when supplied with the same amount of sgRNA, cardiac muscle shows better editing efficacy than skeletal muscle. In addition, on the basis of previous reports, it is likely that AAV9 has better tropism for heart tissue than skeletal muscle (*27*).

Using a single sgRNA against a sequence within exon 45, we observed a high fraction of single nucleotide insertions immediately adjacent to the DNA cut, and these insertions were most commonly an adenosine, corresponding to the next nucleotide adjacent to the site of the initial double-strand DNA break. We made similar observations with single-cut gene editing of exon 51 in mice and dogs lacking exon 50 (*11*). Because cutting with Cas9 has a propensity for a single nucleotide 5′ overhang four nucleotides 5′ to the cut site, the presence of a thymidine at this position favors the insertion of an adenosine on the complementary strand during DNA repair (*28*). This single nucleotide insertion has the potential to restore the open reading frame if the exon is out of frame with the preceding exon by a single nucleotide, as in the case of exons 43 and 45. However, this strategy is less likely to restore the open reading frame if two nucleotides are required to reframe the protein due to the low frequency of two-nucleotide insertions after non-homologous end joining (NHEJ). Nevertheless, deletions that remove the splice acceptor or donor sequence of the out-of-frame exon can restore dystrophin in such cases. Notably, we observed a low frequency of integration of AAV ITR sequences at the site of Cas9 cutting in vivo, as observed by previous reports (*29*, *30*).

Our results highlight the effectiveness of single-cut CRISPR gene editing for efficient restoration of dystrophin in vivo. While several studies have also shown that the use of two sgRNAs to mediate Cas9 cutting at distal genomic sites can allow for excision of large intervening genomic regions and restoration of dystrophin expression from mutant alleles (*31*–*33*), the efficiency of the double-cut approach is low and is associated with unpredictable genomic rearrangements that we have not observed using only a single sgRNA to direct Cas9 cutting. Thus, we believe that the single-cut CRISPR editing approach represents the most viable clinical approach for correction of dystrophin mutations by gene editing. Of course, it also remains to be determined if the marked effects we have observed here in mice can be scaled up to humans with much larger muscles over a longer time frame.

There are several limitations of our study that should be considered. While we have shown marked restoration of dystrophin protein and muscle structure within 4 weeks of AAV delivery, we do not yet know whether these effects will be sustained or, alternatively, may fade over time. Considering that the majority of cardiomyocytes do not turn over, we expect that the benefits of dystrophin restoration in the heart will be lifelong. However, it remains to be determined if there will be gradual turnover of skeletal muscle following delivery of gene editing components by AAV9. In this regard, Wagers and co-workers have reported that AAV9 infects satellite cells in vivo (*34*), which could provide a sustained reservoir of cells for long-term maintenance of dystrophin expression. However, we and others have not observed efficient AAV infection of satellite cells in vivo (*11*, *35*). Whether this represents technical differences in delivery approaches remains to be determined.

Possible immunological responses to Cas9 or dystrophin also remain to be investigated over the long term. While we have not observed an immune response to AAV or Cas9, nor to dystrophin, in our previous studies (*11*), it is conceivable that such responses might be seen over longer time periods. Last, we have tested for possible off-target

genomic cutting at sites predicted to have highest homology with the sgRNAs used to correct the ΔEx44 deletion but have not observed any off-target cutting above background. There has been little evidence of off-target effects of CRISPR-Cas9 editing in mice, other than one report that was retracted (*36*).

In summary, the ΔEx44 DMD mice described here, combined with the optimized ssgRNA and AAV vectors for delivery, should facilitate progress toward long-term correction of dystrophin mutations in mice as a prelude to possible clinical translation.

MATERIALS AND METHODS

Study design

This study was designed with the primary aim to identify the most efficient way to correct an exon 44 mutation in a mouse model of DMD and human patient with DMD–derived iPSCs. Secondary objectives were to investigate the amount of exon skipping, expression of dystrophin protein, and various indicators of disease progression in corrected DMD mice. Peripheral blood mononuclear cells (PBMCs) from healthy individuals and patients with DMD were generated at the UT Southwestern Wellstone Myoediting Core. PBMCs of male donors were used in all experiments. PBMCs were collected on the basis of the mutation of the patients; we did not use exclusion, randomization, or blinding approaches to select the donors. Animal work described in this manuscript has been approved and conducted under the oversight of the UT Southwestern Institutional Animal Care and Use Committee. Animals were allocated to experimental groups based on genotype; we did not use exclusion, randomization, or blinding approaches to assign the animals for the experiments. AAV injection and dissection experiments were conducted in a nonblinded fashion. Blinding approaches were used during grip strength tests, histology validation, immunostaining analysis, CK analysis, and muscle electrophysiology. For each experiment, sample size reflects the number of independent biological replicates and was provided in the figure legends.

Plasmids and cloning

The pSpCas9(BB)-2A-GFP (PX458) plasmid contained the human codon optimized *Sp*Cas9 gene with 2A-EGFP. pSpCas9(BB)-2A-GFP (PX458) was a gift from F. Zhang (Addgene plasmid; catalog no. 48138) (*21*). Cloning of sgRNA was done using Bbs I sites. The sgRNAs in this study, listed in table S1, were selected using prediction of crispr.mit.edu. sgRNA sequences were cloned into PX458 and then tested in tissue culture using human embryonic kidney (HEK) 293 cells and 10T½ cells, as previously described (*37*).

The AAV TRISPR-sgRNAs-CK8e-GFP plasmid contained three sgRNAs driven by the U6, H1, or 7SK promoter and green florescent protein (GFP) driven by the CK8e regulatory cassette. The TRISPR backbone cloning system relies on two consecutive steps of the Golden Gate Assembly (New England Biolabs). Details of the assembly were previously described (*11*).

Human iPSC maintenance and nucleofection

Human iPSCs were cultured in mTeSR™1 media (STEMCELL Technologies) and passaged approximately every 4 days (1:12 to 1:18 split ratio depending on the cell lines). One hour before nucleofection, iPSCs were treated with 10 μM ROCK inhibitor (Y-27632) and dissociated into single cells using Accutase (Innovative Cell Technologies Inc.). iPSCs (1×10^6) were mixed with 5 μg of PX458-sgRNA-2A-GFP plasmid and nucleofected using the P3 Primary Cell 4D-Nucleofector X Kit (Lonza) according to the manufacturer's protocol. After nucleofection, iPSCs were cultured in mTeSR™1 media supplemented with 10 μM ROCK inhibitor and changed to mTeSR™1 media the next day. Three days after nucleofection, media were changed into mTeSR™1 media supplemented with 10 μM ROCK inhibitor and Primosin (100 μg/ml) (InvivoGen) 1 hour before fluorescence-activated cell sorting (FACS). GFP(+) and (−) cells were sorted by FACS and subjected to T7E1 assay. Single clones derived from GFP(+) iPSCs were picked and sequenced.

Human iPSC-CM differentiation

Human iPSCs were cultured in mTeSR™1 media for 3 to 4 days until they reached 90 to 95% confluence. To differentiate the iPSCs into cardiomyocytes, the cells were cultured in CDM3-C media for 2 days, followed by CDM3-WNT media for 2 days, followed by BASAL media for 6 days, followed by SELECTIVE media for 10 days and, last, by BASAL media for 2 to 6 days. Then, the cardiomyocytes were dissociated using TrypLE Express media (Gibco) and replated at 2×10^6 cells per well in a six-well dish. The contents of the differentiation medium can be found in table S1.

Mice

Mice were housed in a barrier facility with a 12-hour light/dark cycle and maintained on standard chow (2916 Teklad Global). ΔEx44 DMD mice were generated in the C57BL/6J background using the CRISPR-Cas9 system. Two sgRNAs specific to the intronic regions surrounding exon 44 of the mouse *Dmd* locus were cloned into vector PX458 (Addgene plasmid; catalog no. 48138) using the primers from table S1. For the in vitro transcription of sgRNA, T7 promoter sequence was added to the sgRNA template by PCR using the primers from table S1. The gel-purified PCR products were used as template for in vitro transcription using the MEGAshortscript T7 Kit (Life Technologies). sgRNAs were purified by MEGAclear Kit (Life Technologies) and eluted with nuclease-free water (Ambion). The concentration of guide RNA was measured by a NanoDrop instrument (Thermo Fisher Scientific). Injection procedures were performed as described previously (*38*). ΔEx44 DMD mice were backcrossed with C57BL/6J mice for more than three generations. ΔEx44 DMD mice and WT littermates were genotyped using primers encompassing the targeted region from table S1. Tail biopsies were digested in 100 μl of 25 mM NaOH, 0.2 mM EDTA (pH 12) for 20 min at 95°C. Tails were briefly centrifuged, followed by addition of 100 μl of 40 mM tris-HCl (pH 5), and mixed to homogenize. Two milliliters of this reaction was used for subsequent PCRs with the primers in table S1, followed by gel electrophoresis.

Genomic DNA isolation, PCR amplification, and T7E1 analysis of PCR products

Genomic DNA of mouse 10T½ fibroblasts, mouse C2C12 myoblasts, human HEK 293 cells, and human iPSCs was isolated using DirectPCR (cell) lysis reagent (VIAGEN) according to the manufacturer's protocol. Genomic DNA of mouse muscle tissues was isolated using GeneJET genomic DNA purification kit (Thermo Fisher Scientific) according to the manufacturer's protocol. Genomic DNA was PCR amplified using GoTaq DNA polymerase (Promega) or with primers. PCR products were gel purified and subcloned into pCRII-TOPO vector (InvitroGen) according to the manufacturer's protocol. Individual clones were

picked, and the DNA was sequenced. Primer sequences are listed in table S1.

Mismatched duplex DNA was obtained by denaturing/renaturing of 25 μl of the genomic PCR product using the following conditions: 95°C for 5 min, 95° to 85°C (−2.0°C/s), 85° to 25°C (−0.1°C/s), hold at 4°C. Then, 25 μl of the mismatched duplex DNA was incubated with 2.7 μl of 10× NEB buffer 2 and 0.3 μl of T7E1 (New England BioLabs) at 37°C for 90 min. The T7E1-digested PCR product was analyzed by 2% agarose gel electrophoresis.

AAV vector production

AAVs were prepared by Boston Children's Hospital Viral Core, as previously described (*39*). AAV vectors were purified by discontinuous iodixanol gradients (Cosmo Bio, AXS-1114542-5) and then concentrated with Millipore Amicon filter unit (UFC910008, 100 kDa). AAV titers were determined by qPCR assays. Briefly, 4 μl of the AAV vector was treated with deoxyribonuclease (DNase) I (NEB M0303S) and 2 M NaOH followed by neutralization. The mixture was serial diluted, and qPCRs were performed with the primers listed in table S1. The number of copies was determined by a standard curve made by serial dilutions of the transgene plasmid.

AAV9 delivery to ΔEx44 DMD mice

Before AAV9 injections, the ΔEx44 DMD mice were anesthetized. For intramuscular injection, the TA muscle of P12 male ΔEx44 DMD mice was injected with 50 μl of AAV9 (1×10^{12} vg/ml) preparations or with saline solution. For intraperitoneal injection, the P4 ΔEx44 DMD mice were injected using an ultrafine needle (31 gauge) with 80 μl of AAV9 preparations with a dosage of 5×10^{13} vg/kg of AAV-Cas9 and a corresponding ratio of AAV-G6 indicated in the figure legend or with saline solution.

Dystrophin Western blot analysis

For Western blot of iPSC-CMs, 2×10^6 cardiomyocytes were harvested and lysed with lysis buffer [10% SDS, 62.5 mM tris (pH 6.8), 1 mM EDTA, and protease inhibitor]. For Western blot of skeletal or heart muscles, tissues were crushed into fine powder using a liquid nitrogen-frozen crushing apparatus. Cell or tissue lysates were passed through a 25-gauge syringe and then a 27-gauge syringe, 10 times each one. Protein concentration was determined by BCA assay, and 50 μg of total protein was loaded onto a 4 to 20% acrylamide gel. Gels were run at 100 V for 15 min and switched to 200 V for 45 min, followed by a 1-hour 20-min transfer to a polyvinylidene difluoride (PVDF) membrane at 100 V at 4°C. The blot was incubated with mouse antidystrophin antibody (MANDYS8, Sigma-Aldrich, D8168), mouse anti-Cas9 antibody (Clone 7A9, Millipore, MAC133), or rabbit anti-GFP antibody (InvitroGen, A-11122) at 4°C overnight, and then with goat antimouse horseradish peroxidase (HRP) antibody or goat anti-rabbit HRP antibody (Bio-Rad Laboratories) at room temperature for 1 hour. The blot was developed using Western Blotting Luminol Reagent (Santa Cruz, sc-2048). The loading control was determined by blotting with mouse anti-vinculin antibody (Sigma-Aldrich, V9131).

Amplicon deep sequencing analysis

PCR of genomic DNA and cDNA from muscles was performed using primers designed against the respective target region and the top 10 off-target sites. A second round of PCR was used to add Illumina flow cell binding sequences and target-specific barcodes on the 5′ end of the primer sequence. All primer sequences are listed in table S1. Before sequencing, DNA libraries were analyzed using a Bioanalyzer High Sensitivity DNA Analysis Kit (Agilent). Library concentration was then determined by qPCR using a KAPA Library Quantification Kit for Illumina platforms. The resulting PCR products were pooled and sequenced with 300-bp paired-end reads on an Illumina MiSeq instrument. Samples were demultiplexed according to assigned barcode sequences. FASTQ format data were analyzed using the CRISPResso software package version 1.0.8.

Histological analysis of muscles

Skeletal muscles from WT and ΔEx44 DMD mice were individually dissected and cryoembedded in a 1:2 volume mixture of Gum Tragacanth powder (Sigma-Aldrich) to Tissue Freezing Medium (Triangle Bioscience). All embeds were snap frozen in isopentane heat extractant supercooled to −155°C. Resulting blocks were stored at −80°C prior to sectioning. Eight-micrometer transverse sections of the skeletal muscle and frontal sections of the heart were prepared on a Leica CM3050 cryostat and air dried prior to staining on the same day. H&E staining was performed according to established staining protocols (*38*), and dystrophin immunohistochemistry was performed using MANDYS8 monoclonal antibody (Sigma-Aldrich) with modifications to the manufacturer's instructions. In brief, cryostat sections were thawed and rehydrated/delipidated in 1% Triton/phosphate-buffered saline, pH 7.4 (PBS). Following delipidation, sections were washed free of Triton, incubated with mouse immunoglobulin G (IgG) blocking reagent (M.O.M. Kit, Vector Laboratories), washed, and sequentially equilibrated with M.O.M. protein concentrate/PBS, and MANDYS8 diluted 1:1800 in M.O.M. protein concentrate/PBS. Following overnight primary antibody incubation at 4°C, sections were washed, incubated with M.O.M. biotinylated anti-mouse IgG, washed, and detection completed with incubation of Vector fluorescein-avidin DCS. Nuclei were counterstained with propidium iodide (Molecular Probes) prior to cover slipping with Vectashield.

For Picrosirius red staining, cryosections of the heart and skeletal muscle, cut at 8-μm thickness, were thawed to room temperature and postfixed in 10% neutral-buffered formalin. Sections were rinsed in tap water before sensitization in heated Bouin's fixative (90 min at 60°C; Polysciences, Warrington, PA). Following tap water rinse, nuclei were counterstained with heated Weigert's iron hematoxylin. Following another tap water rinse, sections were stained with 0.1% Sirius red solution prepared in saturated aqueous picric acid for 1 hour. Sections were destained to collagen specificity with two washes of 0.5% glacial acetic acid, dehydrated, cleared, and coverslips were applied with permanent synthetic mounting media.

Isolated EDL muscle preparation and electrophysiology stimulation

Muscle preparation was performed as described previously (*38*). Briefly, the muscles were surgically isolated from 4-week-old mice and mounted on Grass FT03.C force transducers connected to a Powerlab 8/SP data acquisition unit (AD Instruments, Colorado Springs, CO), bathed in physiological salt solution at 37°C, and gassed continuously with 95% O_2–5% CO_2. After calibration, muscles were adjusted to initial length at which the passive force was 0.5 g and then stimulated with two platinum wire electrodes to establish optimal length (Lo) for obtaining maximal isometric tetanic tension step by step following the protocol (at 150 Hz for 2 s). Specific force

(mN/mm^2) was calculated to normalize contraction responses to tissue cross-sectional area.

Statistics

All data are presented as mean ± SEM. One-way analysis of variance (ANOVA) was performed followed by Newman-Keuls post hoc test for multiple comparisons. Unpaired two-tailed Student's *t* tests were performed for comparison between the respective two groups (WT and ΔEx44 DMD mice, WT and ΔEx44 DMD-AAV9–treated mice, and ΔEx44 DMD control and ΔEx44 DMD-AAV9–treated mice). Data analyses were performed with statistical software (GraphPad Prism Software, San Diego, CA, USA). *P* values less than 0.05 were considered statistically significant.

SUPPLEMENTARY MATERIALS

Supplementary material for this article is available at http://advances.sciencemag.org/cgi/content/full/5/3/eaav4324/DC1

Fig. S1. Analysis of sgRNAs that target the splice acceptor or donor sites for exons 43 and 45.
Fig. S2. Characterization of the ΔEx44 mouse line.
Fig. S3. Intramuscular AAV9 delivery of gene editing components rescues dystrophin expression.
Fig. S4. Analysis of top 10 potential off-target sites.
Fig. S5. Correction of ΔEx44 mice by systemic delivery of AAV9 expressing gene editing components.
Fig. S6. Western blot analysis of corrected ΔEx44 mice by systemic delivery of AAV9 expressing gene editing components.
Fig. S7. Histology of ΔEx44 mice after systemic delivery of AAV9 expressing gene editing components.
Fig. S8. Quantification of histological improvement and qPCR analysis of corrected ΔEx44 DMD mice.
Fig. S9. Histological analysis showing dystrophin restoration in the EDL muscle of corrected ΔEx44 DMD mice.
Table S1. Primer sequences and media components.

REFERENCES AND NOTES

1. E. P. Hoffman, R. H. Brown Jr., L. M. Kunkel, Dystrophin: The protein product of the duchenne muscular dystrophy locus. *Cell* **51**, 919–928 (1987).
2. A. H. Ahn, L. M. Kunkel, The structural and functional diversity of dystrophin. *Nat. Genet.* **3**, 283–291 (1993).
3. K. P. Campbell, S. D. Kahl, Association of dystrophin and an integral membrane glycoprotein. *Nature* **338**, 259–262 (1989).
4. C. L. Bladen, D. Salgado, S. Monges, M. E. Foncuberta, K. Kekou, K. Kosma, H. Dawkins, L. Lamont, A. J. Roy, T. Chamova, V. Guergueltcheva, S. Chan, L. Korngut, C. Campbell, Y. Dai, J. Wang, N. Barišić, P. Brabec, J. Lahdetie, M. C. Walter, O. Schreiber-Katz, V. Karcagi, M. Garami, V. Viswanathan, F. Bayat, F. Buccella, E. Kimura, Z. Koeks, J. C. van den Bergen, M. Rodrigues, R. Roxburgh, A. Lusakowska, A. Kostera-Pruszczyk, J. Zimowski, R. Santos, E. Neagu, S. Artemieva, V. M. Rasic, D. Vojinovic, M. Posada, C. Bloetzer, P.-Y. Jeannet, F. Joncourt, J. Díaz-Manera, E. Gallardo, A. A. Karaduman, H. Topaloğlu, R. El Sherif, A. Stringer, A. V. Shatillo, A. S. Martin, H. L. Peay, M. I. Bellgard, J. Kirschner, K. M. Flanigan, V. Straub, K. Bushby, J. Verschuuren, A. Aartsma-Rus, C. Béroud, H. Lochmüller, The TREAT-NMD DMD Global Database: Analysis of more than 7,000 duchenne muscular dystrophy mutations. *Hum. Mutat.* **36**, 395–402 (2015).
5. L. Echevarría, P. Aupy, A. Goyenvalle, Exon-skipping advances for Duchenne muscular dystrophy. *Hum. Mol. Genet.* **27**, R163–R172 (2018).
6. J. S. Charleston, F. J. Schnell, J. Dworzak, C. Donoghue, S. Lewis, L. Chen, G. D. Young, A. J. Milici, J. Voss, U. DeAlwis, B. Wentworth, L. R. Rodino-Klapac, Z. Sahenk, D. Frank, J. R. Mendell, Eteplirsen treatment for Duchenne muscular dystrophy. *Neurology* **90**, e2146–e2154 (2018).
7. Y. Takeshima, M. Yagi, Y. Okizuka, H. Awano, Z. Zhang, Y. Yamauchi, H. Nishio, M. Matsuo, Mutation spectrum of the dystrophin gene in 442 Duchenne/Becker muscular dystrophy cases from one Japanese referral center. *J. Hum. Genet.* **55**, 379–388 (2010).
8. I. Vieitez, P. Gallano, L. González-Quereda, S. Borrego, I. Marcos, J. M. Millán, T. Jairo, C. Prior, J. Molano, M. J. Trujillo-Tiebas, J. Gallego-Merlo, M. García-Barcina, M. Fenollar, C. Navarro, Mutational spectrum of Duchenne muscular dystrophy in Spain: Study of 284 cases. *Neurología* **32**, 377–385 (2017).
9. K. M. Flanigan, D. M. Dunn, A. von Niederhausern, P. Soltanzadeh, E. Gappmaier, M. T. Howard, J. B. Sampson, J. R. Mendell, C. Wall, W. M. King, A. Pestronk, J. M. Florence, A. M. Connolly, K. D. Mathews, C. M. Stephan, K. S. Laubenthal, B. L. Wong, P. J. Morehart, A. Meyer, R. S. Finkel, C. G. Bonnemann, L. Medne, J. W. Day, J. C. Dalton, M. K. Margolis, V. J. Hinton; the United Dystrophinopathy Project Consortium, R. B. Weiss, Mutational spectrum of DMD mutations in dystrophinopathy patients: Application of modern diagnostic techniques to a large cohort. *Hum. Mutat.* **30**, 1657–1666 (2009).
10. R. Guo, G. Zhu, H. Zhu, R. Ma, Y. Peng, D. Liang, L. Wu, *DMD* mutation spectrum analysis in 613 Chinese patients with dystrophinopathy. *J. Hum. Genet.* **60**, 435–442 (2015).
11. L. Amoasii, C. Long, H. Li, A. A. Mireault, J. M. Shelton, E. Sanchez-Ortiz, J. R. McAnally, S. Bhattacharyya, F. Schmidt, D. Grimm, S. D. Hauschka, R. Bassel-Duby, E. N. Olson, Single-cut genome editing restores dystrophin expression in a new mouse model of muscular dystrophy. *Sci. Transl. Med.* **9**, eaan8081 (2017).
12. L. Amoasii, J. C. W. Hildyard, H. Li, E. Sanchez-Ortiz, A. Mireault, D. Caballero, R. Harron, T.-R. Stathopoulou, C. Massey, J. M. Shelton, R. Bassel-Duby, R. J. Piercy, E. N. Olson, Gene editing restores dystrophin expression in a canine model of Duchenne muscular dystrophy. *Science* **362**, 86–91 (2018).
13. D. G. Allen, N. P. Whitehead, S. C. Froehner, Absence of dystrophin disrupts skeletal muscle signaling: Roles of Ca^{2+}, reactive oxygen species, and nitric oxide in the development of muscular dystrophy. *Physiol. Rev.* **96**, 253–305 (2015).
14. D. G. Allen, N. P. Whitehead, S.C. Froehner, Absence of Dystrophin Disrupts Skeletal Muscle Signaling: Roles of Ca^{2+}, Reactive Oxygen Species, and Nitric Oxide in the Development of Muscular Dystrophy. *Physiological Reviews* **96**, 253 (2015).
15. C.-H. Lau, Y. Suh, In vivo genome editing in animals using AAV-CRISPR system: Applications to translational research of human disease. *F1000Res.* **6**, 2153 (2017).
16. J. R. Mendell, S. al-Zaidy, R. Shell, W. D. Arnold, L. R. Rodino-Klapac, T. W. Prior, L. Lowes, L. Alfano, K. Berry, K. Church, J. T. Kissel, S. Nagendran, J. L'Italien, D. M. Sproule, C. Wells, J. A. Cardenas, M. D. Heitzer, A. Kaspar, S. Corcoran, L. Braun, S. Likhite, C. Miranda, K. Meyer, K. D. Foust, A. H. M. Burghes, B. K. Kaspar, Single-dose gene-replacement therapy for spinal muscular atrophy. *N. Engl. J. Med.* **377**, 1713–1722 (2017).
17. C. Zincarelli, S. Soltys, G. Rengo, J. E. Rabinowitz, Analysis of AAV serotypes 1-9 mediated gene expression and tropism in mice after systemic injection. *Mol. Ther.* **16**, 1073–1080 (2008).
18. H. Büning, L. Perabo, O. Coutelle, S. Quadt-Humme, M. Hallek, Recent developments in adeno-associated virus vector technology. *J. Gene Med.* **10**, 717–733 (2008).
19. M. Martari, A. Sagazio, A. Mohamadi, Q. Nguyen, S. D. Hauschka, E. Kim, R. Salvatori, Partial rescue of growth failure in Growth Hormone (GH)-deficient mice by a single injection of a double-stranded adeno-associated viral vector expressing the GH gene driven by a muscle-specific regulatory cassette. *Hum. Gene Ther.* **20**, 759–766 (2009).
20. F. Schmidt, J. Beaudouin, K. Börner, D. Grimm, 117. AAV-TRISPR – A Novel Versatile AAV vector kit for combinatorial CRISPR and RNAi expression. *Mol. Ther.* **23**, S48–S49 (2015).
21. F. A. Ran, P. D. Hsu, J. Wright, V. Agarwala, D. A. Scott, F. Zhang, Genome engineering using the CRISPR-Cas9 system. *Nat. Protoc.* **8**, 2281–2308 (2013).
22. M. Neri, S. Torelli, S. Brown, I. Ugo, P. Sabatelli, L. Merlini, P. Spitali, P. Rimessi, F. Gualandi, C. Sewry, A. Ferlini, F. Muntoni, Dystrophin levels as low as 30% are sufficient to avoid muscular dystrophy in the human. *Neuromuscul. Disord.* **17**, 913–918 (2007).
23. T. Aslesh, R. Maruyama, T. Yokota, Skipping multiple exons to treat DMD—Promises and challenges. *Biomedicine* **6**, E1 (2018).
24. M. Jinek, F. Jiang, D. W. Taylor, S. H. Sternberg, E. Kaya, E. Ma, C. Anders, M. Hauer, K. Zhou, S. Lin, M. Kaplan, A. T. Iavarone, E. Charpentier, E. Nogales, J. A. Doudna, Structures of Cas9 Endonucleases Reveal RNA-Mediated Conformational Activation. *Science* **343**, 1247997 (2014).
25. M. Jinek, K. Chylinski, I. Fonfara, M. Hauer, J. A. Doudna, E. Charpentier, A programmable dual-RNA–guided DNA endonuclease in adaptive bacterial immunity. *Science* **337**, 816–821 (2012).
26. X. Qi, L. Dong, C. Liu, L. Mao, F. Liu, X. Zhang, B. Cheng, C. Xie, Systematic identification of endogenous RNA polymerase III promoters for efficient RNA guide-based genome editing technologies in maize. *Crop J.* **6**, 314–320 (2018).
27. C. Zincarelli, S. Soltys, G. Rengo, W. J. Koch, J. E. Rabinowitz, Comparative cardiac gene delivery of adeno-associated virus serotypes 1–9 reveals that AAV6 mediates the most efficient transduction in mouse heart. *Clin. Transl. Sci.* **3**, 81–89 (2010).
28. B. R. Lemos, A. C. Kaplan, J. E. Bae, A. E. Ferrazzoli, J. Kuo, R. P. Anand, D. P. Waterman, J. E. Haber, CRISPR/Cas9 cleavages in budding yeast reveal templated insertions and strand-specific insertion/deletion profiles. *Proc. Natl. Acad. Sci. U.S.A.* **115**, E2040–E2047 (2018).
29. A. Donsante, D. G. Miller, Y. Li, C. Vogler, E. M. Brunt, D. W. Russell, M. S. Sands, AAV Vector integration sites in mouse hepatocellular carcinoma. *Science* **317**, 477 (2007).
30. A. Barzel, N. K. Paulk, Y. Shi, Y. Huang, K. Chu, F. Zhang, P. N. Valdmanis, L. P. Spector, M. H. Porteus, K. M. Gaensler, M. A. Kay, Promoterless gene targeting without nucleases ameliorates haemophilia B in mice. *Nature* **517**, 360–364 (2015).
31. N. E. Bengtsson, J. K. Hall, G. L. Odom, M. P. Phelps, C. R. Andrus, R. D. Hawkins, S. D. Hauschka, J. R. Chamberlain, J. S. Chamberlain, Muscle-specific CRISPR/Cas9 dystrophin gene editing ameliorates pathophysiology in a mouse model for Duchenne muscular dystrophy. *Nat. Commun.* **8**, 14454 (2017).

32. C. E. Nelson, C. H. Hakim, D. G. Ousterout, P. I. Thakore, E. A. Moreb, R. M. C. Rivera, S. Madhavan, X. Pan, F. A. Ran, W. X. Yan, A. Asokan, F. Zhang, D. Duan, C. A. Gersbach, In vivo genome editing improves muscle function in a mouse model of Duchenne muscular dystrophy. *Science* **351**, 403–407 (2016).
33. D. G. Ousterout, A. M. Kabadi, P. I. Thakore, W. H. Majoros, T. E. Reddy, C. A. Gersbach, Multiplex CRISPR/Cas9-based genome editing for correction of dystrophin mutations that cause duchenne muscular dystrophy. *Nat. Commun.* **6**, 6244–6244 (2015).
34. M. Tabebordbar, K. Zhu, J. K. W. Cheng, W. L. Chew, J. J. Widrick, W. X. Yan, C. Maesner, E. Y. Wu, R. Xiao, F. A. Ran, L. Cong, F. Zhang, L. H. Vandenberghe, G. M. Church, A. J. Wagers, In vivo gene editing in dystrophic mouse muscle and muscle stem cells. *Science* **351**, 407–411 (2016).
35. A. L. H. Arnett, P. Konieczny, J. N. Ramos, J. Hall, G. Odom, Z. Yablonka-Reuveni, J. R. Chamberlain, J. S. Chamberlain, Adeno-associated viral vectors do not efficiently target muscle satellite cells. *Mol. Ther. Methods Clin. Dev.* **1**, 14038 (2014).
36. K. A. Schaefer, W.-H. Wu, D. F. Colgan, S. H. Tsang, A. G. Bassuk, V. B. Mahajan, Unexpected mutations after CRISPR–Cas9 editing in vivo. *Nat. Methods* **14**, 547–548 (2017).
37. C. Long, H. Li, M. Tiburcy, C. Rodriguez-Caycedo, V. Kyrychenko, H. Zhou, Y. Zhang, Y.-L. Min, J. M. Shelton, P. P. A. Mammen, N. Y. Liaw, W.-H. Zimmermann, R. Bassel-Duby, J. W. Schneider, E. N. Olson, Correction of diverse muscular dystrophy mutations in human engineered heart muscle by single-site genome editing. *Sci. Adv.* **4**, eaap9004 (2018).
38. C. Long, L. Amoasii, A. A. Mireault, J. R. McAnally, H. Li, E. Sanchez-Ortiz, S. Bhattacharyya, J. M. Shelton, R. Bassel-Duby, E. N. Olson, Postnatal genome editing partially restores dystrophin expression in a mouse model of muscular dystrophy. *Science* **351**, 400–403 (2016).
39. J. C. Grieger, V. W. Choi, R. J. Samulski, Production and characterization of adeno-associated viral vectors. *Nat. Protoc.* **1**, 1412–1428 (2006).

Acknowledgments: We thank J. Cabrera for graphics, C. Nolen for technical assistance, D. Tennison for genotyping, V. S. Malladi for bioinformatic analysis, Neuro-Models Facility and L. Ingle for grip strength experiments, Flow Cytometry Core and A. Mobley for FACS, C. Wang and the Boston Children's Hospital Viral Core for AAV production, D. Caballero for qPCR analysis, E. Sanchez-Ortiz for assistance in the Western blot, and C. Long, Y. Zhang, V. Kyrychenko, and N. Jones for the constructive advice. We are grateful to S. Hauschka (University of Washington) for the CK8e regulatory cassette and to D. Grimm (Heidelberg University Hospital, Germany) for the TRISPR plasmid. **Funding:** This work was supported by the NIH (grants HL130253 and AR-067294), the Senator Paul D. Wellstone Muscular Dystrophy Cooperative Research Center (grant U54 HD 087351), the Parent Project Muscular Dystrophy Award, CureDuchenne, Exonics Therapeutics, and the Robert A. Welch Foundation (grant 1-0025 to E.N.O.). **Author contributions:** Y.-L.M., R.B.-D., and E.N.O. wrote and edited the manuscript. Y.-L.M. designed the experiments and performed the animal studies, iPSCs studies, genomic DNA, T7E1 assays, RT-PCR, Western blots, muscle electrophysiology, and analysis. H.L. performed the genomic, RT-PCR, and off-target analyses. C.R.-C performed the iPSC culture. A.A.M. performed the tissue processing experiments. J.H. performed the muscle electrophysiology analysis. J.M.S. performed immunohistochemistry and H&E staining. J.R.M. performed the zygote injection to generate the mice. L.A. provided assistance and advice. P.P.A.M. provided blood samples and oversight of the electrophysiology analysis. **Competing interests:** R.B.-D and E.N.O. are consultants for Exonics Therapeutics. L.A. is an employee of Exonics Therapeutics. Y.-L.M., R.B.-D., and E.N.O. are co-inventors on a patent application related to this work (U.S. patent application number 15/914,728), regarding the mouse model and strategy presented in this study. The other authors declare that they have no competing interests. **Data and materials availability:** All data needed to evaluate the conclusions in the paper are present in the paper and/or the Supplementary Materials. Additional data related to this paper may be requested from the authors. The pSpCas9(BB)-2A-GFP (PX458) plasmid can be provided by Addgene pending scientific review and a completed material transfer agreement. Requests for the pSpCas9(BB)-2A-GFP (PX458) plasmid should be submitted to Addgene.

Submitted 14 September 2018
Accepted 28 January 2019
Published 6 March 2019
10.1126/sciadv.aav4324

Citation: Y.-L. Min, H. Li, C. Rodriguez-Caycedo, A. A. Mireault, J. Huang, J. M. Shelton, J. R. McAnally, L. Amoasii, P. P. A. Mammen, R. Bassel-Duby, E. N. Olson, CRISPR-Cas9 corrects Duchenne muscular dystrophy exon 44 deletion mutations in mice and human cells. *Sci. Adv.* **5**, eaav4324 (2019).